Transactions on Machine Intelligence 3(3) (2020) 176-190

ISSN Online: 2821-1693

Transactions on Machine Intelligence

Journal Homepage: https://tmachineintelligence.ir/index.php/TMI

A Novel Multifunctional Multi-Port Integrated Converter for Fuel-Cell Hybrid Electric Vehicles

H. Soltani Gohari[1,*], K. Abbaszadeh[2]

[1] Department of Electrical Engineering, K.N.Toosi University of Technology, Tehran, Iran
[2] Professor, Department of Electrical Engineering, K.N.Toosi University of Technology, Tehran, Iran

ARTICLE INFO

Article History:
Received 3 May 2020
Received in revised form 11 June 2020
Accepted 21 September 2020
Available online 21 September 2020

Keywords:
On-Board Charger, Fuel Cell Hybrid EV, Integrated Converter, Multi-Port Converter, Active And Reactive Power, Regenerative Braking Energy, Energy Management Strategy

ABSTRACT

The effective design of the powertrain for Fuel Cell Hybrid Electric Vehicles (FCHEVs) holds paramount importance in achieving high efficiency. Traditional FCHEV powertrains typically employ separate converters, a configuration that adversely impacts overall system efficiency. This paper presents a novel approach by proposing a multifunctional multi-port integrated converter designed for fuel cell-based hybrid electric vehicles. Specifically, the converter is tailored for FCHEVs incorporating an ultra-capacitor and a battery alongside the fuel cell stack to enhance system efficiency and dynamic response during startup. The versatility of the proposed converter is evident in its ability to operate in three distinct modes: battery charging, propulsion, and regenerative braking. Notably, the regenerative braking mode facilitates the return of energy to the battery, optimizing its state of charge (SOC). A standout feature of this converter is its capacity to charge the battery with a pure sinusoidal input current and controllable active and reactive power. This capability arises from its unique topology and the detailed control strategy elucidated in this paper. To complement the converter's performance, an energy management strategy is introduced, contributing to its efficient operation. The topology, coupled with the control strategy, is rigorously simulated using MATLAB/SIMULINK, with results affirming the thoroughness of the system analysis.

1. INTRODUCTION

Growing concerns about environmental pollution, coupled with the notable impact of fossil fuel-based vehicles, have spurred an increased adoption of electric vehicles (EVs) and Hybrid EVs [1]. Fuel cell hybrid EVs (FCHEVs) emerge as a viable solution for environmental issues, given their operation without pollution. The incorporation of additional power sources such as batteries or ultra-capacitors serves to enhance the startup dynamics and overall efficiency of vehicles relying solely on fuel cells. Key components of FCHEVs' powertrain include their charger and the DC-DC converter, which interfaces between the power sources and the motor drive system, significantly influencing vehicle operation and efficiency [2-5].

* Corresponding Author: Hsoltani@email.kntu.ac.ir
Department of Electrical Engineering, K.N.Toosi University of Technology, Tehran, Iran

http://dx.doi.org/10.47176/TMI.2020.176

The convergence of the charger and DC-DC converter can substantially improve the overall system efficiency by reducing component count and increasing power density [6]. Beyond the tasks of charging and propulsion, the converter should also efficiently handle the duty of returning regenerative braking energy to the battery. This function is crucial for storing regenerative energy, employing dynamic braking, and maintaining the battery's state of charge (SOC) within a specific range. Dynamic braking offers advantages over traditional mechanical braking methods.

While existing converters, such as the one introduced in [7], can charge the battery and return regenerative energy, they lack applicability in FCHEVs. Similarly, the converter proposed in [8] operates solely in charging and propulsion modes. Chargers presented in [9-10] require an external circuit for propulsion and regenerative braking, leading to increased weight and reduced efficiency. Additionally, converters introduced in [11-12] focus on charging the battery and lack the capability to function as a DC-DC converter or return regenerative energy.

In this paper a multi-input integrated converter is introduced which can work in five different operating modes. It can work as a charger (mode1) with controllable active and reactive power depending on smart grid commands or costumer requirements due to the control strategy which is introduced in this paper. This converter has three propulsion modes which are:

Mode2: FC + UC + Battery

Mode3: FC + UC

Mode4: FC

An exceptionally effective power management strategy is presented in this context, allowing for the meticulous control of the output power from each source. This strategy is tailored to consider the state of charge (SOC), voltage, and current of the battery, as well as the fuel cell (FC) and ultra-capacitor (UC). By leveraging this comprehensive information, the power management system optimizes the performance of each source, ensuring an efficient and balanced utilization of resources. Furthermore, the proposed converter exhibits the capability to operate in regenerative mode (mode 5), enabling the simultaneous return of regenerative energy to the battery and the charging of the battery using both regenerative energy and FC-generated energy. This dual functionality enhances the converter's versatility and contributes to the overall efficiency of the hybrid system.

For a clearer understanding of the converter's operation, please refer to Figure 1, where the various operation modes are elucidated. This visual representation serves as a valuable guide in comprehending the distinct functionalities and transitions within the converter, offering a comprehensive overview of its operation.

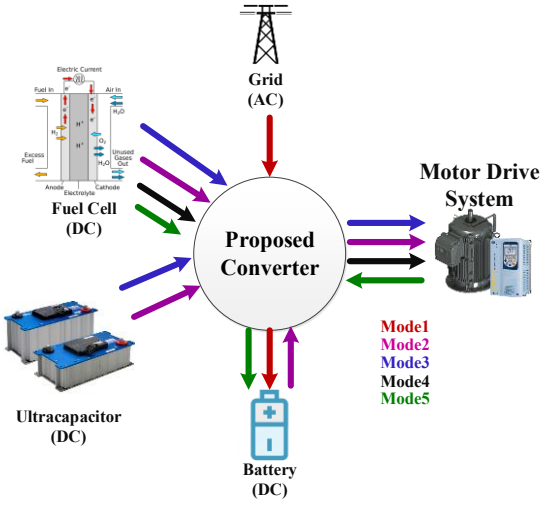

Fig. 1. Operation Modes of proposed converter

2. PROPOSED CONVERTER

2.1. Topology

As illustrated in Figure 2, the proposed converter operates as a two-stage converter. The primary function of the first stage involves rectifying the grid voltage while allowing for controllable active and reactive power. The subsequent stage, referred to as the multi-input DC-DC stage or the second stage, is responsible for regulating different voltages to ensure the generation of an appropriate output voltage.

Adapting to various vehicle conditions, such as Charging, Propulsion, and Regenerative Braking, the proposed converter is capable of functioning in five distinct operation modes:

Charging Battery (Mode 1): In this mode, the converter focuses on charging the battery.

Propulsion with Three Sources (Mode 2): The converter operates to facilitate propulsion using all three power sources concurrently.

Propulsion with Two Sources (Mode 3): This mode involves propulsion with a selective combination of two power sources.

Propulsion with One Source (Mode 4): The converter propels the vehicle using a single power source.

Returning Braking Energy to Battery and Charging Battery with FC (Mode 5): This mode is dedicated to returning braking energy to the battery and simultaneously charging the battery using energy from the fuel cell (FC).

These distinct operation modes showcase the converter's adaptability and versatility, allowing it to dynamically respond to varying vehicle requirements and optimizing its performance accordingly.

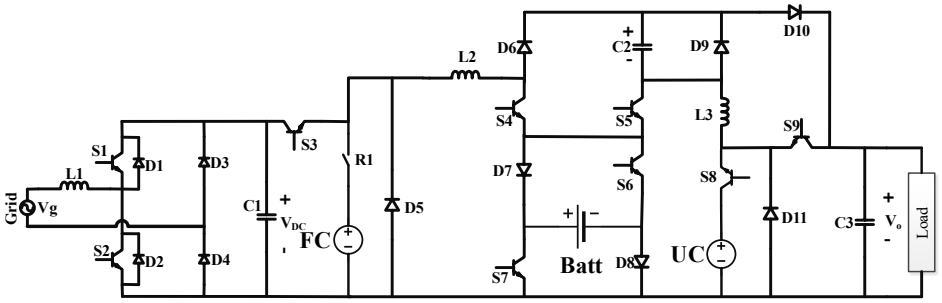

Fig. 2. Structure of proposed converter

2.2. Operation and Steady State Analysis

As mentioned above, this converter has different switching patterns in operating modes which are explained in detail in the next parts:

2.2.1. Mode1 (Charging)

During this mode, the battery undergoes charging through the utilization of grid voltage facilitated by the AC-DC stage. Initially, the AC-DC stage rectifies the grid voltage with a pure sinusoidal input current, directing the energy towards charging the DC-Link capacitor (C1). The operational status of the switches within the AC-DC stage is categorized into two conditions based on the sign of the grid voltage. Fig.3 provides a visual representation of the switch status and current paths during both the positive and negative half-cycles of the grid voltage. Notably, during the positive half-cycle, S2 is engaged in high-frequency operation, while in the negative half-cycle, S1 takes on this high-frequency operation.

Subsequently, the DC-DC stage functions as a buck converter, facilitating the transfer of energy to charge the battery. Fig.4 delineates the primary components of the converter in this mode and illustrates the paths of current

during this charging process. This mode represents an efficient approach to harnessing grid voltage for the purpose of recharging the battery, and the detailed schematic provides insights into the intricate workings of the converter during this specific operation.

State1 (0<t<DTs): in this state S3 and S4 are ON and D7 and D8 are directly biased so the L2 is magnetized by (VDC-VBatt) [Fig.4 (a)].

State2 (DTs<t<Ts): at the begging of this state S3 is turned OFF and D5 is directly biased consequently. So L2 is demagnetized by (-VBatt) [Fig.4 (b)].

From KVL identities, the voltages across inductive component L2 is obtained as:

$$L2: D(VDC - VBatt) + (1 - D)(-VBatt) = 0. \quad (1)$$

So the voltage gain can be obtained as:

$$VBatt = DVDC. \quad (2)$$

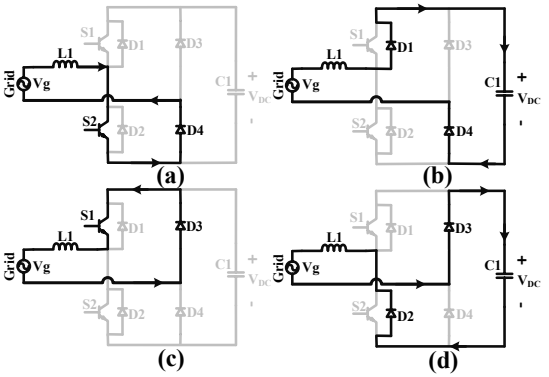

Fig. 3. Current paths in AC-DC stage in mode1 (a) and (b) Vg>0 (c) and (d) Vg<0

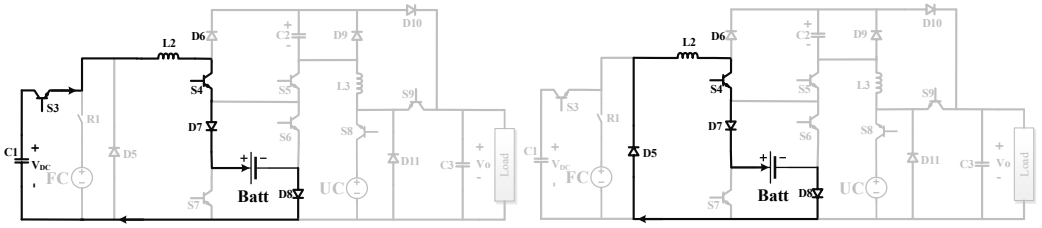

Fig. 4. Current paths in DC-DC stage in mode1 (a) state1 (b) state2

2.2.2. Mode2 (propulsion with all sources)

This mode is selected when all sources have the ability to deliver power. In this mode, the AC-DC stage does not have any task. Switching cycle of this mode is divided into four states:

State1 (0<t<D1Ts): in this state S4, S5, S6, S7, and S8 are ON so L2 and L3 are charged by (VFC+VBatt) and (VUC+VBatt), respectively [Fig.5 (a)].

State2 (D1Ts<t<D2Ts): at t=D1Ts S6 is turned OFF so D7 is directly biased. In this interval L2 and L3 are charged by (VFC) and (VUC), respectively [Fig.5 (b)].

State3 (D2Ts<t<D3Ts): in this time interval the L2 needs to be demagnetized so S4 is turned OFF and L2 is discharged by (VFC-VC2). The L3 keeps charging by VUC [Fig.5 (c)].

State4 (D3Ts<t<Ts): by turning the S4 ON and turning the S5 OFF the L2 is magnetized by (VFC) and C3 is charged by the energy of C2 and L3 [Fig.5 (d)].

From KVL identities, the voltages across inductive components L2, L3 ,and also C2 are obtained as:

$$\begin{cases} L2: D1(VFC + VBatt) + D2(VFC) + D3(VFC - VC2) + (1 - D1 - D2 - D3)(VFC) = 0 \\ C2: VC2 = \frac{VFC + D1VBatt}{D3} \\ L3: D1(VUC + VBatt) + D2(VUC) + D3(VUC) + (1 - D1 - D2 - D3)(VUC + VC2 - Vo) = 0 \end{cases} \quad (3)$$

So the voltage gain can be obtained as:

$$Vo = \frac{VBatt(D1 - D1^2 + D1D2) + D3VUC + VFC(1 - D1D2 - D3)}{D3(1 - D1 - D2 - D3)}. \quad (4)$$

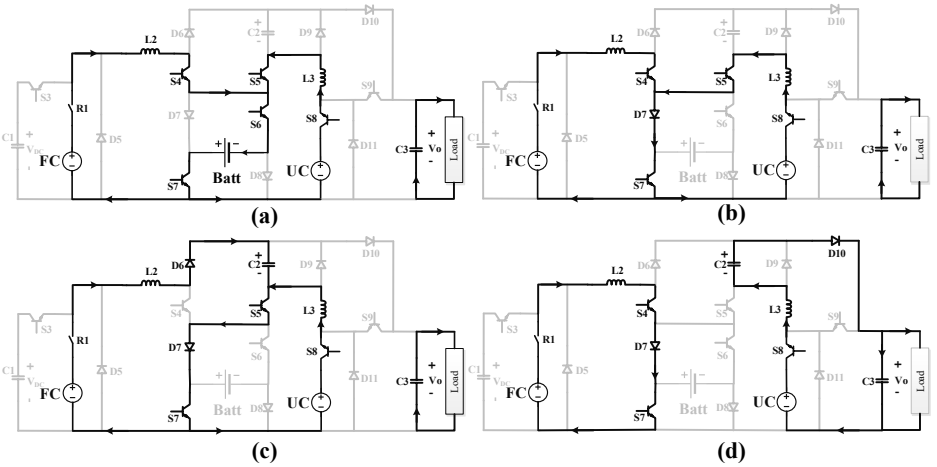

Fig. 5. Current paths in DC-DC stage in mode2 (a) state1 (b) state2 (c) state3 (d) state4

2.2.3. Mode3 (propulsion with two sources)

From KVL identities, the voltages across inductive components L2, L3 ,and also C 2 are obtained as:

$$\begin{cases} L2: D1(VFC) + D2(VFC - VC2) + (1 - D1 - D2)(VFC) = 0 \\ C2: VC2 = \frac{VFC}{D2} \\ L3: D1(VUC) + D2(VUC) + (1 - D1 - D2)(VUC + VC2 - Vo) = 0 \end{cases} \quad (5)$$

So the voltage gain can be obtained as:

$$Vo = \frac{VUC(D2 - D1D2) + VFC(1 + D1D2 - D2 - D1)}{D2(1 - D1 - D2)} \quad (6)$$

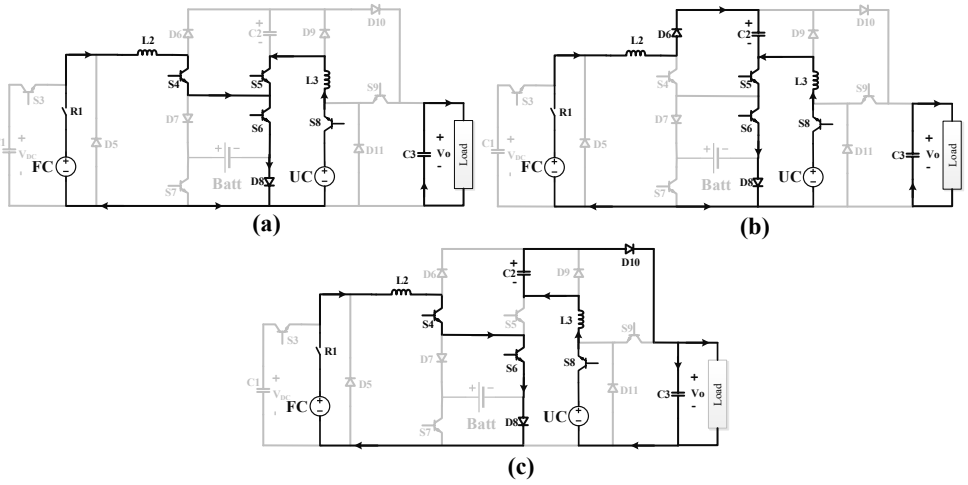

Fig. 6. Current paths in DC-DC stage in mode3 (a) state1 (b) state2 (c) state3

2.2.4. Mode4 (propulsion with FC)

If the voltage of UC meets its minimum allowed value the converter has to handles the load with FC. Working in this mode has two states:

State1 (0<t<DTs): first S4 and S7 are ON so L2 is magnetized by (VFC) [Fig.7 (a)].

State2 (DTs<t<Ts): at t=DTs S4 is turned OFF so C3 is charged by energy of L2 [Fig.7 (b)].

From KVL identities, the voltages across inductive component L2 is obtained as:

$$L2: D(VFC) + (1 - D)(VFC - V0) = 0 \tag{7}$$

So the voltage gain can be obtained as:

$$Vo = \frac{VFC}{1-D} \tag{8}$$

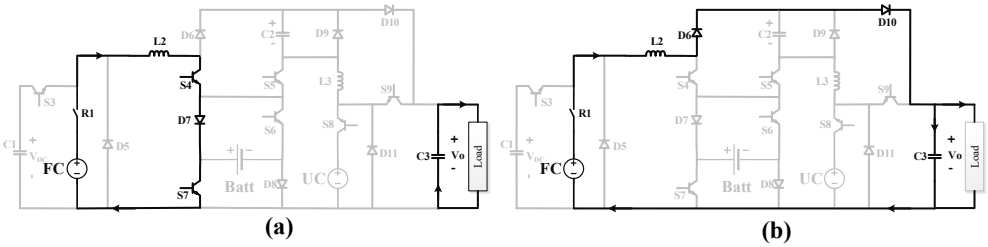

Fig. 7. Current paths in DC-DC stage in mode4 (a) state1 (b) state2

2.2.5. Mode5 (Braking)

In this mode the converter retuns braking energy to battery and increases the battery SOC by the energy of FC and regenerative energy, simultaneously. In the load side the converter acts as a buck converter and decreased the motor voltage.

State1 (0<t<DTs):in this state S4, S5, S7, and S9 are ON so L2 and L3 are magnetized by (VFC) and (Vo), respectively [Fig.8 (a)].

State2 (DTs<t<Ts): S7 and S9 are turned OFF so D8 and D11 are directly biased so L2 and L3 are demagnetized by (VFC-VBatt) and (-VBatt), respectively, and battery is charged. [Fig.8 (b)].

From KVL identities, the voltages across inductive components L2, L3 are obtained as:

$$\begin{cases} L2: D(VFC) + (1-D)(VFC - VBatt) = 0 \\ L3: D(Vo) + (1-D)(Vo - VBatt) = 0 \end{cases} \quad (9)$$

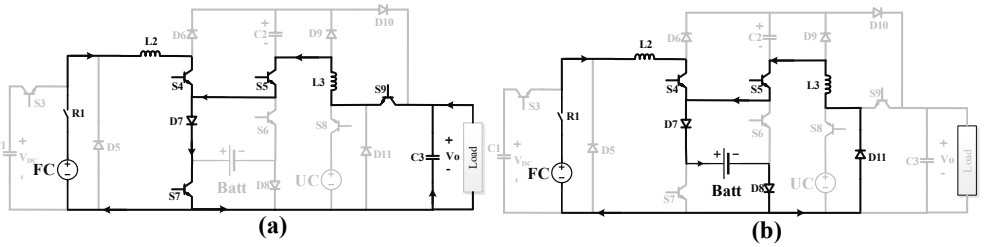

Fig. 8. Current paths in DC-DC stage in mode5 (a) state1 (b) state2

3. CONTROL ALGORITHM

The AC-DC stage of the proposed converter possesses the capability to rectify the grid voltage while offering control over both active and reactive power, in accordance with inputs received from the smart grid or customer specifications. This is made possible through the implementation of a sophisticated control strategy detailed in this section. As depicted in Fig.9, the proposed control method is a dual-loop PI controller, comprising the following components:

Phase-Lock-Loop (PLL): Responsible for acquiring in-phase and quadrature signals of voltage and current.

P-Q Controller: Calculates the required active and reactive power based on the inputs from the PLL.

Reference Current Calculator: Utilizes equations (10)-(12) to generate reference current values.

Gate Signal Generator: Incorporates the generated reference current and the measured input current to compute the error signal. Subsequently, a PI controller is employed in the gate signal generator to regulate the input current. The output signal of this controller is then compared with a 20kHz triangular wave [13].

This comprehensive control approach ensures precise manipulation of the AC-DC stage, allowing for flexibility in adjusting active and reactive power according to the specific demands communicated by the smart grid or end-user preferences. The inclusion of a dual-loop PI controller enhances the converter's responsiveness and accuracy in achieving the desired control objectives.

$$\theta = tan^{-1}\left(\frac{Qref}{Pref}\right). \quad (10)$$

$$Iref = \frac{Pref}{Vg\,Cos(\theta)}. \quad (11)$$

$$iref^{*} = \sqrt{2} Iref\, Sin(wt - \theta). \quad (12)$$

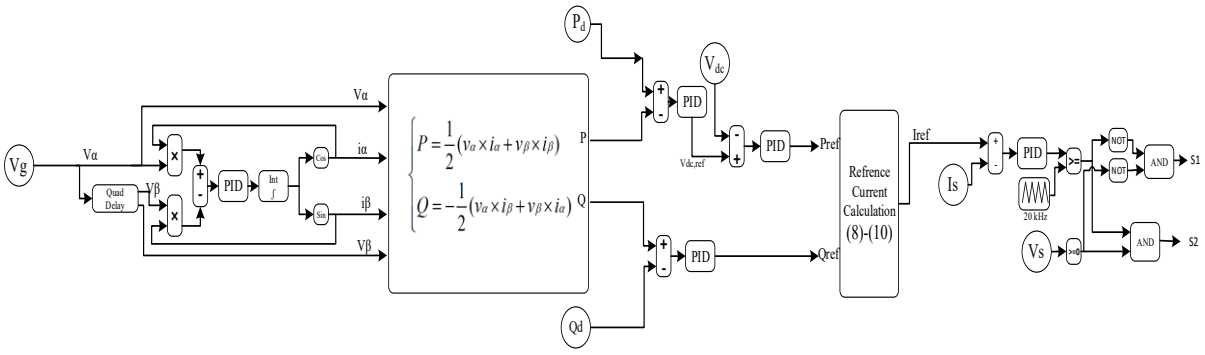

Fig. 9. Proposed control strategy

4. POWER MANAGEMENT

In all Fuel Cell Hybrid Electric Vehicles (FCHEVs), the development of an effective power management controller is imperative for regulating the utilization of energy from each source based on various parameters such as Battery State of Charge (SOC), output voltages of sources, calculated efficiency, and more. This paper introduces a novel power management strategy specifically designed for the proposed converter, wherein operation modes are selected based on the sign of Id (demand current), Battery SOC, voltage of the Ultra-Capacitor (UC), and their respective limits. The detailed flowchart of the proposed power management strategy is illustrated in Fig.10.

Employing this method not only enhances overall system efficiency but also imposes constraints on the Battery SOC, maintaining it within a narrow and specific range. This deliberate restriction contributes to an extended battery life and a reduction in maintenance costs. The meticulous control provided by this power management strategy ensures optimized energy utilization, fostering improved efficiency and longevity of critical components within the FCHEV system.

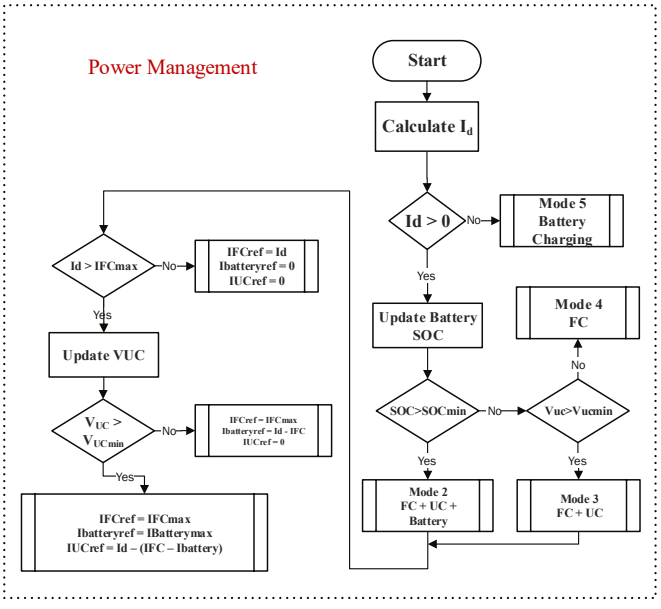

Fig. 10. Power management strategy flowchart

5. SIMULATION

To validate the system analysis, the proposed converter undergoes simulation in MATLAB/SIMULINK, utilizing the values specified in Table 1. For the simulation, the converter is assumed to be connected to the grid with a voltage of Vg=220 rms. The battery configuration employed in this simulation consists of 80V/25Ah cells, with three cells utilized, resulting in a total battery voltage of 240V. The fuel cell stack generates an output voltage of 150V, while an ultra-capacitor with a 100V output voltage is also integrated into the system. Simulations are conducted for all operation modes, and the outcomes are elucidated in the subsequent discussion.

Table 1. The proposed converter specifications

Parameters	Value	Parameters	Value
Input voltage(Vg)	220(rms)	Battery port voltage	240V
DC-link voltage (Vdc)	340 V	L1	5 mH
Motor port voltage (Vo)	600V	L2	0.8 mH
Output Power	2 kW	L3	0.8 mH
Battery cell	80V ; 25Ah	C1	7mF
Battery cells number	3	C2	470µF
Input current THD	5.5 %	C3	1000µF
Fuel cell Voltage	150V	Ultra capacitor voltage	100V

Fig.11-15 are related to the simulation of mode1 in unity power factor condition. Fig.11 shows the grid voltage and input current and their phase angle. As it can be seen, the power factor is more than 0.99. Fig.12 shows the FFT analysis of input current and its THD. In order to show the converter ability to track generated reference input current by controller, reference and measured input current are shown in Fig.13.

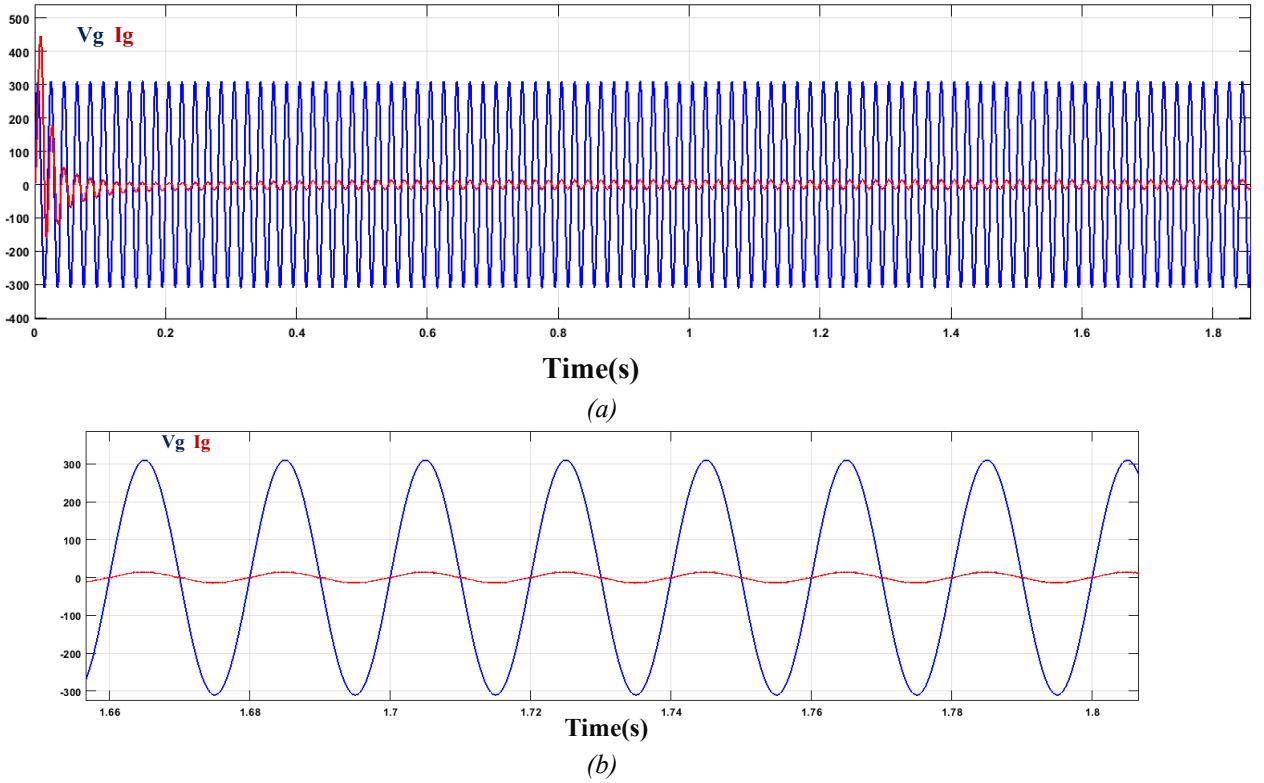

Fig. 11. (a) Grid voltage and input current (b) zoomed version

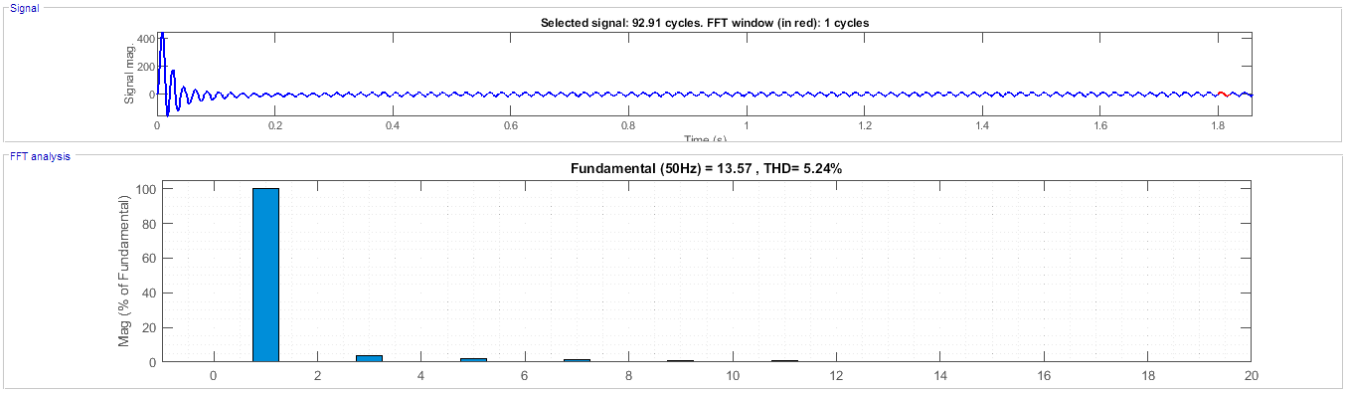

Fig. 12. FFT Analysis of input current

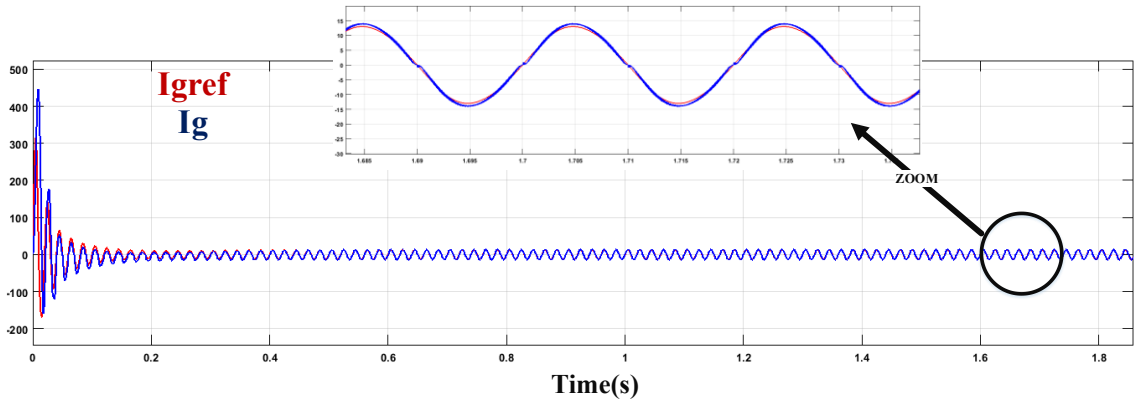

Fig. 13. Reference and measured input current

The stead state of DC-link voltage with its dynamic response is shown in Fig.14.

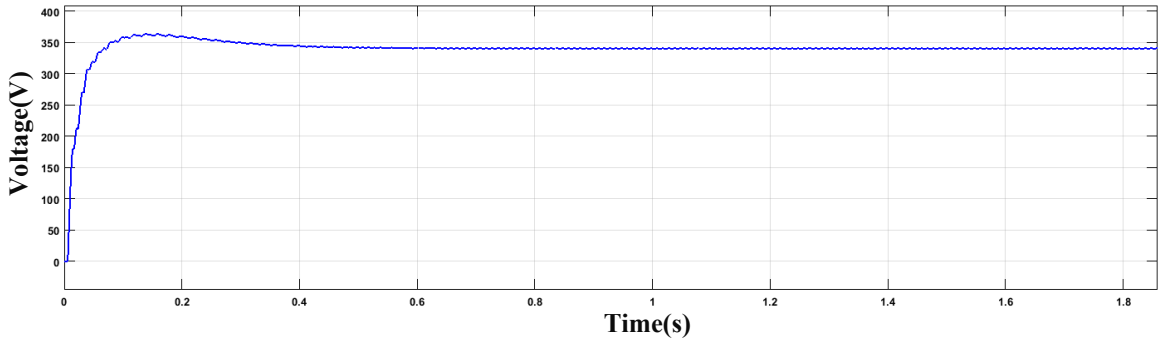

Fig. 14. DC-link voltage

The voltage and current of L2 during mode1 are shown in Fig.15.

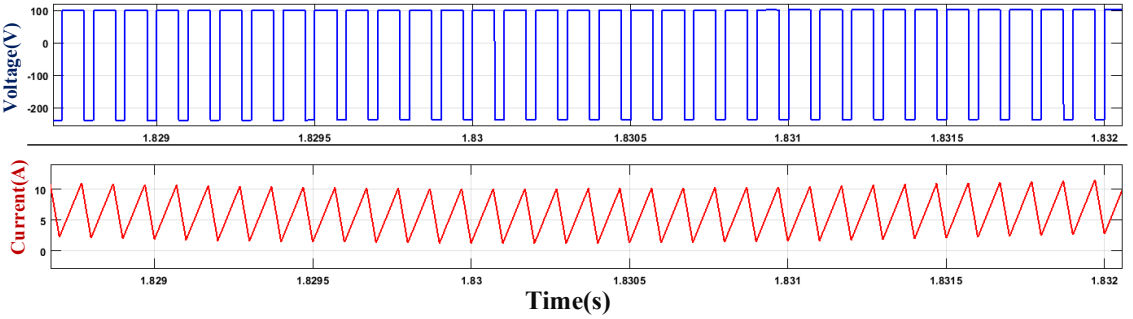

Fig. 15. Voltage and current of L2 in mode1

The output voltage (Vo) in mode2 is shown in Fig.16. As it can be seen, its steady state ripple is less than 2 volts.

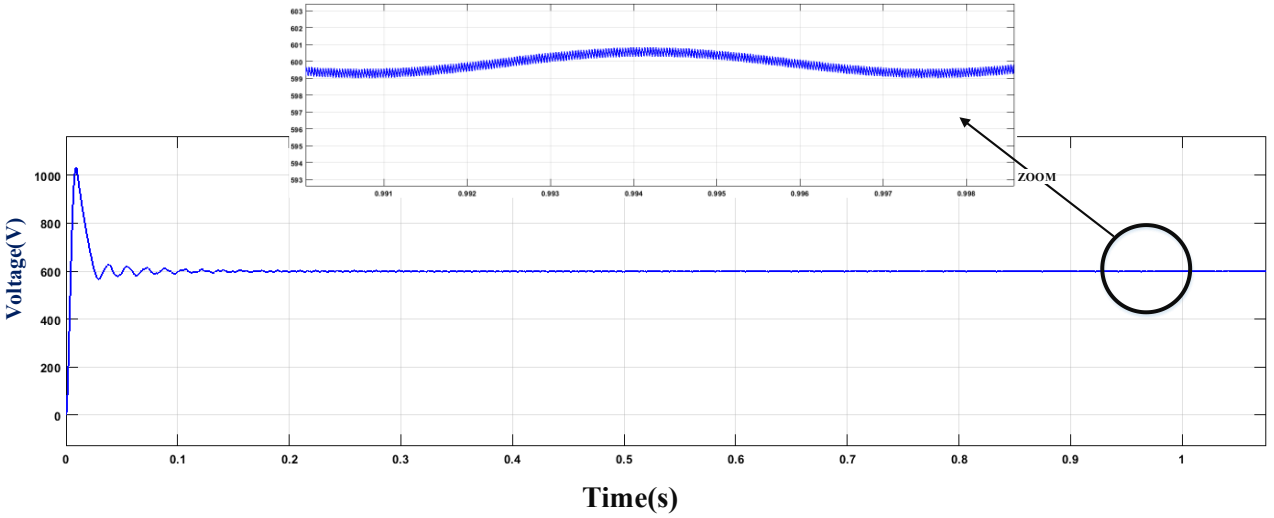

Fig. 16. Output voltage in mode2

Voltage and current of L2 and L3 during mode2 are shown in Fig.17 and Fig.18, respectively, which confirm the system analysis.

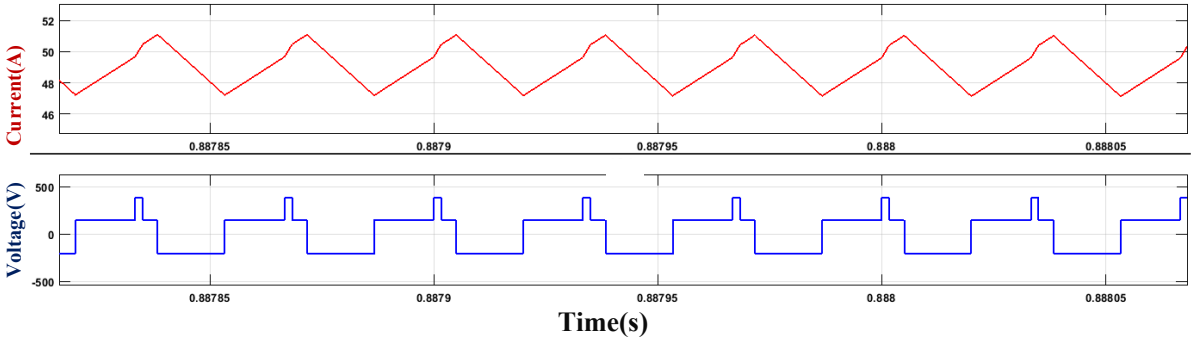

Fig. 17. Voltage and current of L2 in mode2

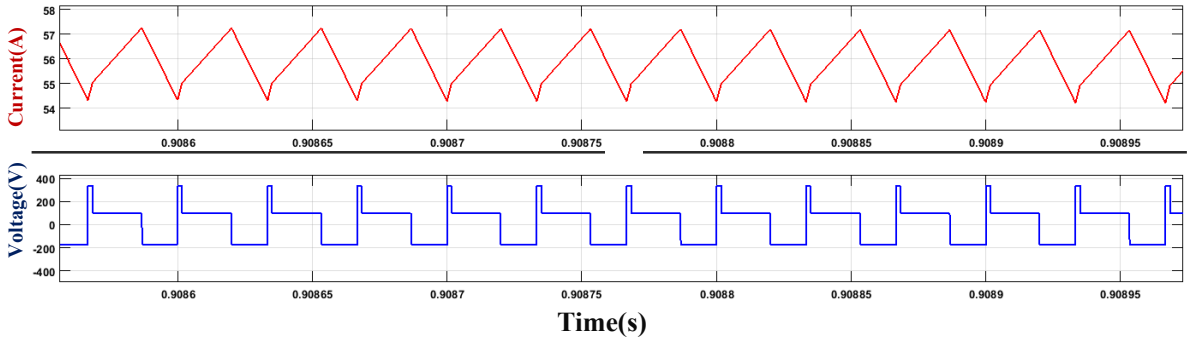

Fig. 18. Voltage and current of L3 in mode2

As shown in Fig.19, the steady state output voltage in mode3 is fixed to its set point (600v) and its ripple is less than 1 volts.

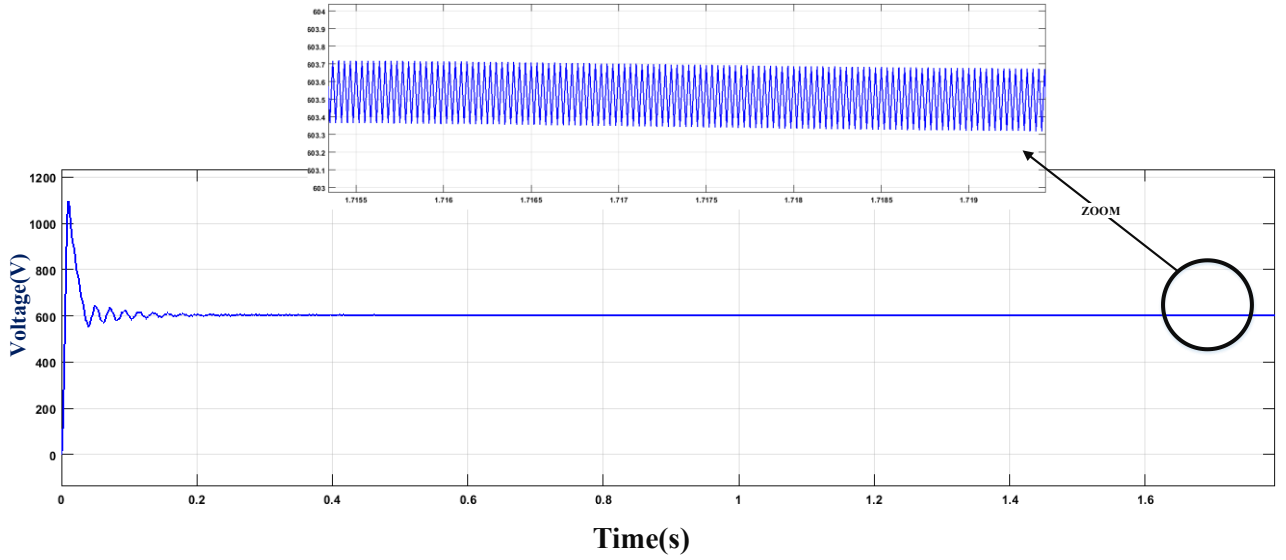

Fig. 19. Output voltage in mode3

Fig.20 and Fig.21 show the voltage and current of L2 and L3 during mode3, respectively.

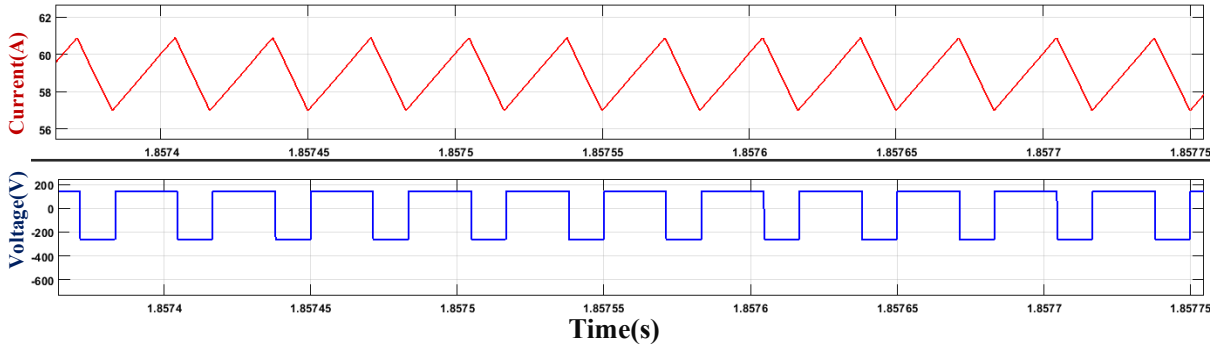

Fig. 20. Voltage and current of L2 in mode3

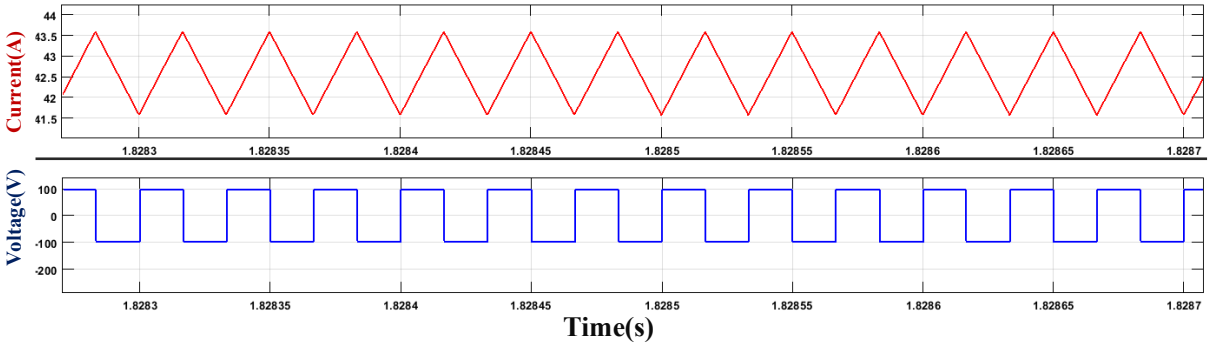

Fig. 21. Voltage and current of L3 in mode3

The regeneration condition is also simulated. Fig.22 shows the battery voltage with its transient state. Fig.23 and Fig.24 show the voltage and current of L2 and L3, respectively.

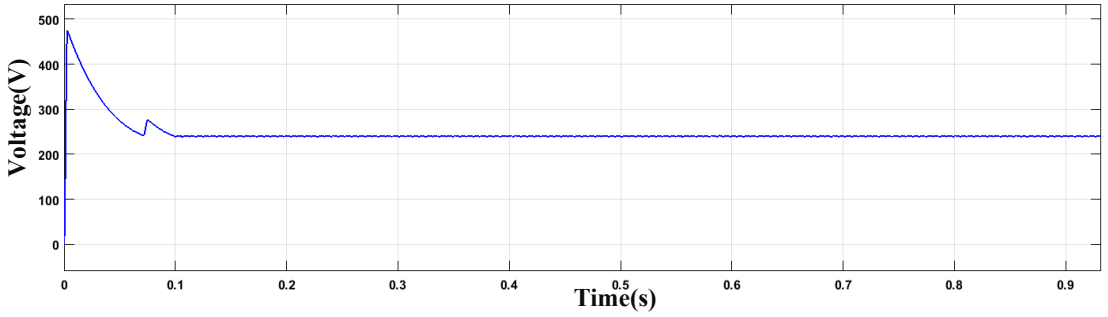

Fig. 22. Battery voltage in mode5

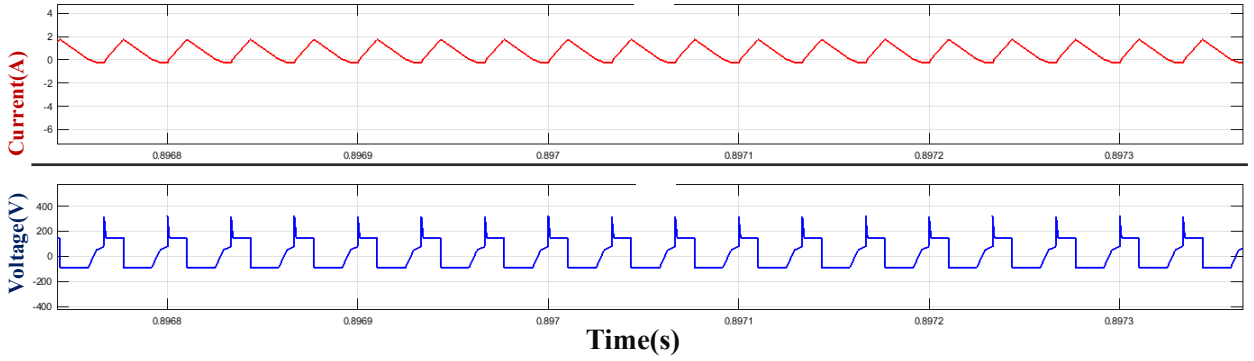

Fig. 23. Voltage and current of L2 in mode5

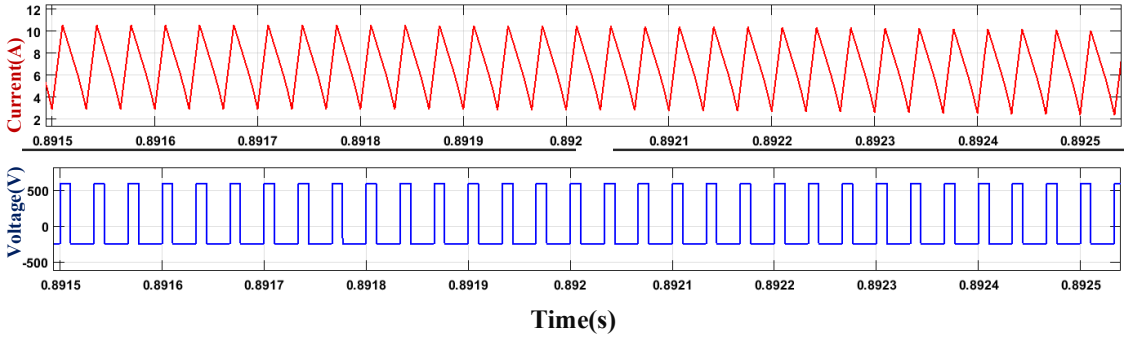

Fig. 24. Voltage and current of L3 in mode5

6. CONCLUSION

The paper introduces a multifunctional multi-port integrated converter designed for application in Fuel Cell Hybrid Electric Vehicles (FCHEVs). This versatile converter demonstrates capability in operating across five distinct modes, each meticulously analyzed and elucidated in the paper. To enhance the Total Harmonic Distortion (THD) of the input current and exercise precise control over active and reactive power during battery charging mode, a robust control strategy is detailed.

Moreover, the paper introduces a valuable and straightforward energy management strategy tailored for FCHEVs. The proposed converter, coupled with the introduced control strategy, undergoes simulation using MATLAB/SIMULINK software. The simulation results are thoroughly analyzed, providing insights into the performance and efficacy of the proposed system. The collective contributions of the multifunctional converter, advanced control strategy, and energy management approach aim to address key challenges in FCHEV systems, as detailed and substantiated through simulation outcomes.

Transparency Statement

The data supporting this study are available upon reasonable request to the corresponding author, subject to ethical and confidentiality considerations.

Acknowledgments

We would like to express our gratitude to all individuals who contributed to this project.

Declaration of Interest

The authors declare that they have no competing interests.

Funding

This research received no specific grant from any funding agency, commercial, or not-for-profit sectors.

REFERENCES

[1] Chan, C. C., & Chau, K. T. (1997). An overview of power electronics in electric vehicles. IEEE Transactions on Industrial Electronics, 44(1), 3–13. https://doi.org/10.1109/41.557493

[2] Emadi, A., Lee, Y. J., & Rajashekara, K. (2008). Power electronics and motor drives in electric, hybrid electric, and plug-in hybrid electric vehicles. IEEE Transactions on Industrial Electronics, 55(6), 2237–2245. https://doi.org/10.1109/TIE.2008.922768

[3] Singh, A. K., & Pathak, M. K. (2016). An improved two-stage non-isolated converter for on-board plug-in hybrid EV battery charger. Proceedings of the IEEE 1st International Conference on Power Electronics, Intelligent Control and Energy Systems (ICPEICES), 1–6. https://doi.org/10.1109/ICPEICES.2016.7853084

[4] Musavi, F., Edington, M., Eberle, W., & Dunford, W. G. (2012). Evaluation and efficiency comparison of front-end AC-DC plug-in hybrid charger topologies. IEEE Transactions on Smart Grid, 3(1), 413–421. https://doi.org/10.1109/TSG.2011.2166413

[5] McGrath, B. P., Holmes, D. G., McGoldrick, P. J., & Galloway, R. (2007). Design of a soft-switched 6-kW battery charger for traction applications. IEEE Transactions on Power Electronics, 22(4), 1136–1144. https://doi.org/10.1109/TPEL.2007.900458

[6] Park, T., & Kim, T. (2013). Novel energy conversion system based on a multimode single-leg power converter. IEEE Transactions on Power Electronics, 28(1), 213–220. https://doi.org/10.1109/TPEL.2012.2195681

[7] Dusmez, S., & Khaligh, A. (2013). A compact and integrated multifunctional power electronic interface for plug-in electric vehicles. IEEE Transactions on Power Electronics, 28(12), 5690–5701. https://doi.org/10.1109/TPEL.2012.2233763

[8] Dusmez, S., & Khaligh, A. (2014). A charge-nonlinear-carrier-controlled reduced-part single-stage integrated power electronics interface for automotive applications. IEEE Transactions on Vehicular Technology, 63(3), 1091–1103. https://doi.org/10.1109/TVT.2013.2284592

[9] Kong, P. Y., Aziz, J. A., Sahid, M. R., et al. (2014). A bridgeless PFC converter for on-board battery charger. Proceedings of the IEEE Conference on Energy Conversion (CENCON), 383–388. https://doi.org/10.1109/CENCON.2014.6967534

[10] Shi, C., Wang, H., Dusmez, S., & Khaligh, A. (2017). A SiC-based high-efficiency isolated onboard PEV charger with ultrawide DC-link voltage range. IEEE Transactions on Industry Applications, 53(1), 501–511. https://doi.org/10.1109/TIA.2016.2605063

[11] Patil, D., Sinha, M., & Agarwal, V. (2012). A Cuk converter-based bridgeless topology for high power factor fast battery charger for electric vehicle application. Proceedings of the IEEE Transportation Electrification Conference & Expo (ITEC), 1–6. https://doi.org/10.1109/ITEC.2012.6243481

[12] Patil, D., & Agarwal, V. (2016). Compact onboard single-phase EV battery charger with novel low-frequency ripple compensator and optimum filter design. IEEE Transactions on Vehicular Technology, 65(4), 1948–1956. https://doi.org/10.1109/TVT.2015.2424927

[13] Gohari, H. S., & Abbaszadeh, K. (2020). A novel controllable bidirectional switching-capacitor based buck-boost charger for EVs. Proceedings of the 2020 11th Power Electronics, Drive Systems, and Technologies Conference (PEDSTC), 1–6. https://doi.org/10.1109/PEDSTC49159.2020.9088502